Received: 15 October 2021 | Revised: 14 November 2021 | Accepted: 01 December 2021
DOI: 10.22034/ecc.2022.310593.1251
Eurasian Chemical Communications
SAMI

FULL PAPER

Synthesis, identification, antibacterial, medical and dying performance studies for azo-sulfamethoxazole metal complexes

Duaa Jameel Jasim* | **Alyaa Khider Abbas**

Department of Chemistry, College of Science, University of Baghdad, Baghdad, Iraq

By diazotization and coupling for 7-Bromo-8-hydroxyquinoline and sulfamethoxazole, the novel [4-(5-(7-Bromo-8-hydroxyquinoline) azo) sulfamethoxazole] (HAS) has been produced. To make new complexes, the ligand (HAS) was reacted with [Pd (II), Pt (II), Ni (II), and Co(II)]. Spectroscopic methods, thermal analysis, molar conductance data, and magnetic measurements were utilized to analyze both the (HAS) ligand and metal complexes of the ligand. The technique of mole ratio was used to determine the stoichiometric of the complexes, which was [1:2] [M:L] for the complexes of Pt(II) and Pd(II) exhibited square planar geometry, whereas Ni(II) was determined to be octahedral and Co(II) was determined to be distorted octahedral geometry. For HAS ligand and its complexes, the dyeing performance, anti-bacterialand and anti-fungal properties were studied. The Platinum complex was also investigated as an antioxidant and anti-cancer agent, whereas cobalt complex was investigated as an anti-inflammatory agent. The ligand was put to the test as an indicator.

***Corresponding Author:**
Duaa Jameel Jasim
Email: duaajameel321@gmail.com, aalyakhider@yahoo.com

KEYWORDS

Sulfamethoxazole; anticancer; antioxidant; dying performance; complexes.

Introduction

A crucial role has been played by azo dyes that contain heterocyclic rings in developing coordination chemistry [1]. Azole chemicals, on the other hand, have been combined with different biological processes, involving RNA, DNA, nitrogen fixation, and cancer [2]. The antibiotic sulfamethoxazole (SMX) is a bacteriostatic agent that is commonly utilized to treat a variety of infections. Its widespread usage in even animals and humans produces unmetabolized and active metabolites with a wide range of biological effects [3]. Sulfamethoxazole (SMX) is a commonly prescribed and utilized antibiotic in both veterinary medicine and human, as well as a common sulfonamide in both aquatic and terrestrial settings. In a European review of pharmaceuticals and personal care products, it was also named to a top ten list of high-priority medications [4]. 8-Hydroxyquinoline compounds have been found to have several antibacterial, antioxidant, anticancer, antiinflammatory, and antineurodegenerative properties. When compared to the original chemical, the halogenated 8HQ, particularly 7-Bromo-8HQ, had a strong antigrowth effect against Gram-negative bacteria [5]. The main goal of our research is to synthesize new complexes of [Ni (II), Co (II), Pt (II), and Pd (II)] with the ligand [4-(5-(7-Bromo-8-hydroxyquinoline) azo) sulfamethoxazole] (HAS). The ligand and its complexes were identified by different physicochemical methods. The antioxidant, anticancer,

antibacterial, antifungal, and anti-inflammatory properties were investigated. In addition, the dying performance and the ability for the ligand to act as an indicator were studied.

Experimental

Instruments and materials

The materials and solvents were used of the highest possible grade. Metal content and elemental analysis for the (HAS) ligand and complexes of the ligand were obtained using (C.H.N.S), and the proportion of metal in complexes was calculated using (Eure EA 3000 Elemental analyzer). FT-IR spectrophotometry was performed using a "Nova 350spectrophotomerer "Flam Atomic Absorption Spectrophotometer. UV-Visible Spectra for all the investigated compounds were recorded on the (SHIMADZU 1800- UV spectrophotometer) using ethanol in the range of (200-1100) nm using the SHIMADZU 8400s spectrophotometer in the region of (250- 4000) cm^{-1} with CsI. The ^{1}HNMR spectra were obtained with tetramethylsilane as the internal standard on a BRUKER AV 400 Advance -III (400 MHz and 100 MHz) equipment. The metal content of the produced ligands and complexes was evaluated by thermal analysis (TG) (SDT Q600 V20.9 Build). Stuart melting point equipment was used to determine the melting points of all the compounds. In ethanol (10^{-3} M), the molar conductance of metal ion complexes was investigated using HI 9811-5" HANNA equipment. The Mohr technique was utilized to determine the chloride content of the materials examined. M.S.B. is the model's name. At room temperature, the magnetic susceptibility of the investigated complexes was evaluated utilizing the Auto Apparatus.

Synthesis of (HAS) ligand (Scheme 1)

The ligand [4-(5-(7-Bromo-8-hydroxyquinoline)azo) sulfamethoxazole] (HAS) was synthesized as described in the literature [6] with minor modifications, as indicated in Scheme 1. The diazonium salt was synthesized by dissolving (2.53 gm; 0.01 mole) sulfamethoxazole in 10 mL deionized water and then adding 10 mL concentrated HCl, then cooled 10% $NaNO_2$ solution was added to the mixture which had been chilled in an ice bath (0°C), with stirring for 1 hour. The solution of diazonium salt was slowly added to an alcoholic alkaline solution of 7-Bromo-8-hydroxyquinoline (2.2 gm; 0.01 mol). After that, the solution's pH was adjusted to (5-6). Leaved it overnight to precipitate, the colored powder that resulted was filtered and dried after washing it by ethanol: deionized water [1:1] and dry.

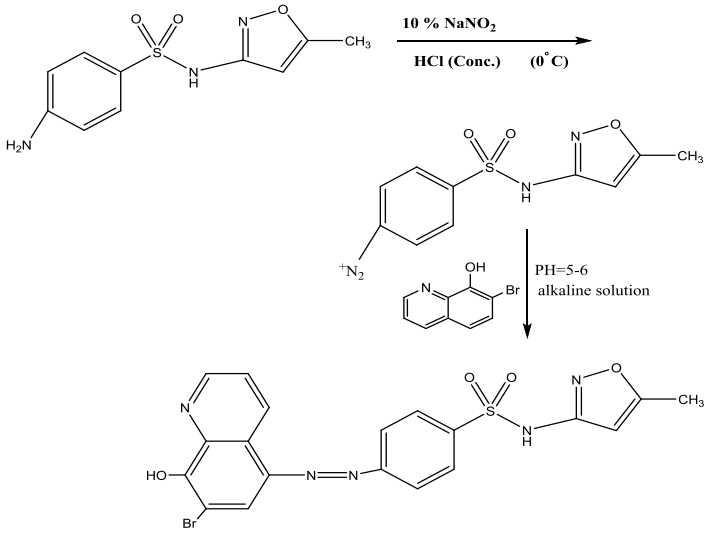

SCHEME 1 Synthesis of (HAS) ligand

Metal complex synthesis

The ligand(HAS) in an ethanolic solution [0.9786 gm,0.002 M] is added to each of the ethanolic solution of the chloride salt for selected metals [Ni (II), Co (II) , Pt(II) and Pd (II)] (0.00l M) (0.237, 0.237,0.410 and 0.177,) gm respectively in terms of mole ratio [1:2] [M:L]. The combination then was refluxed for three hours, and the results were analyzed using a TLC technique. The color precipitate is filtered and rinsed with 100% ethanol many times. It was then allowed to dry. Table 1 appeared properties of the synthesized compound.

TABLE 1 Metal complexes' and physical characteristics and analysis

Compounds (M.wt) (gm/mol)	**M:L**	**The Color λ (nm)**	**% Experimental % (Theoretical)**					**(Λm) ohm^{-1} cm^2 mol^{-1}**
			C	**H**	**N**	**S**	**M**	
HAS($C_{19}H_{14}N_5O_4SBr$) (489.329)	-	Yellow orange (405)	46.87 46.59	2.19 2.86	14.52 14.30	7.11 6.53	-	-
Pt ($C_{38}H_{38}N_{10}O_{13}S_2Br_2$) (1263.74)	1:2	Orange-red (443)	36.54 36.08	3.42 3.00	11.82 11.07	5.45 5.06	15.22 15.43	10.9
Pd ($C_{38}H_{30}N_{10}O_9S_2Br_2$) (1103.078)	1:2	Reddish brown (500)	41.76 41.33	3.12 2.71	12.40 12.69	6.13 5.80	9.86 9.64	19.3
Co ($C_{38}H_{40}N_{10}O_{14}S_2Br_2$) (1145.58)	1:2	Blackish red (496)	40.05 39.80	3.74 3.49	12.58 12.22	5.73 5.58	5.61 5.14	18.5
Ni ($C_{38}H_{40}N_{10}O_{14}S_2Br_2$) (1145.351)	1:2	Orange red (466)	39.62 39.81	3.83 3.49	12.69 12.22	5.64 5.58	5.34 5.12	19.6

Anti-oxidant and radical scavenging activity

To test the reductive ability, 1 mL of each concentration of $[Pt(HAS)_2].5H_2O$ (0.08, 0.16, 0.32, and 0.64 mg/mL). After mixing with 1 mL of 0.2M phosphate buffer (pH 6.6) and 1.5 mL of 1 percent potassium ferricyanide, the mixture was incubated at 50 °C for 20 minutes, as reported in the literature [7]. 1 mL of 10% trichloroacetic acid was added to the liquid to stop the reaction. 2.5 mL of the supernatant, 2 mL distilled water, and 0.5 mL of freshly made, 1 percent ferric chloride, were mixed after centrifugation for 10 minutes at 3000 pm. After that, at 700nm, the absorbance was measured. The Trolox solutions were treated in the same way (standards). All of the tests were carried out in duplicate.

Based on the stable DPPH free radical's scavenging activity, the antioxidant activity of the $[Pt(HAS)_2].5H_2O$ and standard (vitamin C) were evaluated using the technique of [8]. In a test tube, 3.9 mL of DPPH solution was mixed with an aliquot of 0.1 mL of each of the two complexes or standard (0.625, 0.125, 0.250, and 0.500 mg/mL). A spectrophotometer was used to determine the absorbance of each solution at 517 nm after 30 minutes of incubation at 37 °C. Triplicates of all measurements were taken. The following equation was used to calculate the ability to scavenge DPPH radicals:

$$\text{DPPH radical scavenging activity}\,(\%) = \left(1 - \frac{\text{Absorbance of Sample}}{\text{Absorbance of Standard}}\right) \times 100$$

Anticancer effectiveness

The cytotoxic activity and mode of action of synthesized $[Pt(HAS)_2].5H_2O$ complex were studied in this part against liver cancer cell line (HepG-2) and normal cell line (WRL68). MTT assays were used to evaluate $[Pt(HAS)_2].5H_2O$ complex after incubation for 24 at 37 °C with concentrations of (6.25, 12.50, 25, 50, 100, 200 and 400) $\mu g/$ mL. The chosen compound was discovered to have an inhibitory effect on the (HepG-2) and WRL68 cell lines. The extent of the toxic impact was calculated by comparing the percentage of inhibition to the control.

Antibacterial and antifungal of synthesized ligand and its complexes

The efficacy of antibacterial of the new azo ligand (HAS) and complexes of ligand was tested in vitro with two pathogenic microorganisms using a disk diffusion technique in [9] (10^{-3} M) ethanol as a solvent. Inhibitory zones (in mm) were measured after the Petri dishes were incubated for 24 hours at 37 °C (for bacteria) and 72 hours (for fungi), with sulfamethoxazole as a control for bacteria and fluconazole for fungi. The pathogenic microorganisms utilized were chosen because they may cause a wide spectrum of life-threatening disorders in living systems. There were gram-positive bacteria *Staphylococcus aureus (Staph)* and gram-negative bacteria *Escherichia Coli (E.coli)* while there was the one type of fungi (Rhizopus microsporus).

Burns healing (anti-inflammatory)

Burns's healing impact was tested to see if $[Co(HAS)_2(H_2O)_2].4H_2O$ has anti-inflammatory activity. The ability of $[Co(HAS)_2(H_2O)_2].4H_2O$ at (1.5 mM), silver sulfadiazine (positive control), and negative control to heal burns was investigated by determining the number of days required to recover the results.

Dying method

In the wool fabric, the coloring characteristics of the ligand (HAS) and its complexes were used. (0.3 gm) of azo dyes (HAS) ligand and its complexes were dissolved in an ethanolic solution of 10% NaOH, then added 50 mL of distilled water. After that, A piece of clean white wool fabric(10×10) cm, (30 gm ± 3 gm) that soaked in distilled water for (30) minutes was transferred to the azo dye solution and heated to 60 °C for 10 minutes. The soaked cotton fabric piece was washed three times with (250) mL distilled water containing 1 gm of soap to remove any non-reacting species. Finally, dyed raw was dried by hot steam [10].

Acid - base indicator

The ligand (HAS) was employed as an indicator in acid-base titration using (0.1M) HC1 vs (0.1M) NaOH and (0.1M) CH_3COOH versus (0.1M) NaOH. When going from an acidic to a basic solution, the ligand has a distinct color in one solution and a dramatic color change in the other.

Results and discussion

In general, the complexes were created by reacting the desired metal salts with the azo ligand (HAS) at a mole ratio of [1:2] M:L, whereas the ligand was created by diazotizing sulfamethoxazole in acidic circumstances, and then it is paired with the Alkaloid 7-Bromo 8-hydroxyquinoline as a nucleophile. The data was obtained by atomic absorption to identify a percentage of the metal, and elemental analysis was under the usual formulae for the ligand (HAS) and its complexes of metals. All complexes have non-ionic properties (Table 1). In addition, the planned structure is backed up by spectroscopic measurement (FTIR, 1HNMR, and UV- Vis) and thermo-gravimetric analysis (TGA).

The mole ratio

The mole ratio approach was used to evaluate the stoichiometric reaction of the ligand (HAS) and its [Pd (II), Pt (II), Ni (II), and Co(II)] complexes. This is the most well-known approach for determining the type of complexes generated in the solution that requires separation when the amount of ligand is altered (0.25 mL) and the amount of metal ion is kept constant; this technique was utilized to test the absorbance vs molar ratio of the (M:L).[10]

The relationship between the (M:L) ratio and the absorbance is shown in Figure 1, while the results are collected in a Table 2. All synthesized complexes have a (1:2) (M:L) ratio.

TABLE 2 HAS-metal ion solution absorbance vs. mole ratio

M:L	Absorbance			
	Co(HAS)	Ni(HAS)	Pt(HAS)	Pd(HAS)
1:0.25	0.41	0.38	0.11	0.04
1:0.50	0.52	0.41	0.12	0.05
1:0.75	0.65	0.43	0.19	0.08
1:1	0.72	0.49	0.23	0.12
1:1.25	0.85	0.53	0.27	0.16
1:1.50	0.92	0.59	0.31	0.21
1:1.75	0.95	0.62	0.36	0.25
1:2	1.21	0.73	0.43	0.32
1:2.25	1.24	0.72	0.42	0.33
1:2.50	1.25	0.72	0.42	0.32
1:2.75	1.24	0.73	0.41	0.31
1:3	1.23	0.71	0.42	0.32
1:3.25	1.25	0.72	0.43	0.32
1:3.50	1.24	0.73	0.41	0.33
1:3.75	1.25	0.72	0.42	0.32
1:4	1.26	0.72	0.42	0.31

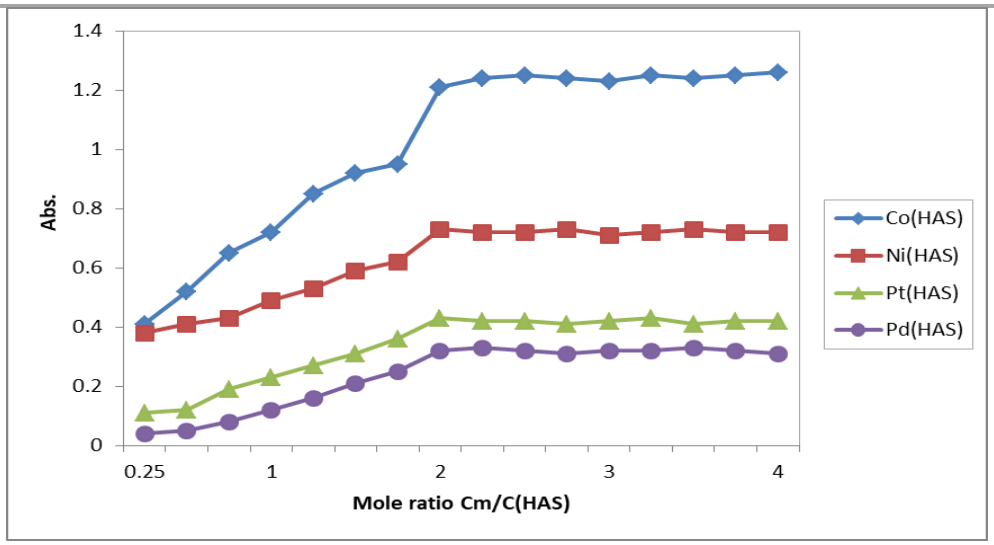

FIGURE 1 The mole ratio of (HAS) ligand and the complexes

Gibbs free energy and stability constant

The stability constant can be calculated spectrophotometrically [11]. For complexes with a mole ratio of [M: L] [1:2] was calculated using the equations below.

$$K = \frac{(1-\alpha)}{4\alpha^3 c^2}$$

$$\alpha = \frac{(Am - As)}{Am}$$

C= (molar concentration) for the complexes in molar (c = 10^{-3}M)

α = degree of disintegration

Am = the solution's absorption which contains (volume of the metal and additional ligand)

As = solution absorption that consists (1:1) stoichiometric (M:L)

From Table (3) the stability increases in the following order : $[Ni(HAS)_2(H_2O)_2].4H_2O$ > $[Co(HAS)_2(H_2O)_2].4H_2O$ > $[Pt(HAS)_2].5H_2O$ > $[Pd(HAS)_2].H_2O$

This equation yielded the thermodynamic characteristics of ΔG (Gibbs free energy). [12]:

ΔG = - RT ln K

Where:

R= constant of gas which equal 8.31 J. $mole^{-1}$. K^{-1}

(T) = Temperature absolute (Kelvin)

At the information we got through ΔG, the synthesis of all complexes was spontaneous. Table 3 shows the behavior of the thermodynamic parameters of ΔG:

TABLE 3 The Gibbs free energy (ΔG) and the stability constant (K) for the synthesized complexes

Complex	As	Am	K	Ln K	ΔG(J/mole)
$[Co(HAS)_2(H_2O)_2].4H_2O$	0.72	1.21	2241431.26	14.62	-36211.17
$[Ni(HAS)_2(H_2O)_2].4H_2O$	0.49	0.73	4760892.67	15.37	-38061.96
$[Pt(HAS)_2].5H_2O$	0.23	0.43	1330283.21	14.10	-34919.19
$[Pd(HAS)_2].H_2O$	0.12	0.32	384000.98	12.85	-31842.28

The FT-IR spectra

The synthesized ligand (HAS) may subsist in two tautomeric variants that are conceivable (azo-hydrazone) as was shown in Scheme 2 and the deprotonation of the hydroxyl moiety in the 7-Bromo 8-HQ for two tautomers leads to anion [13].

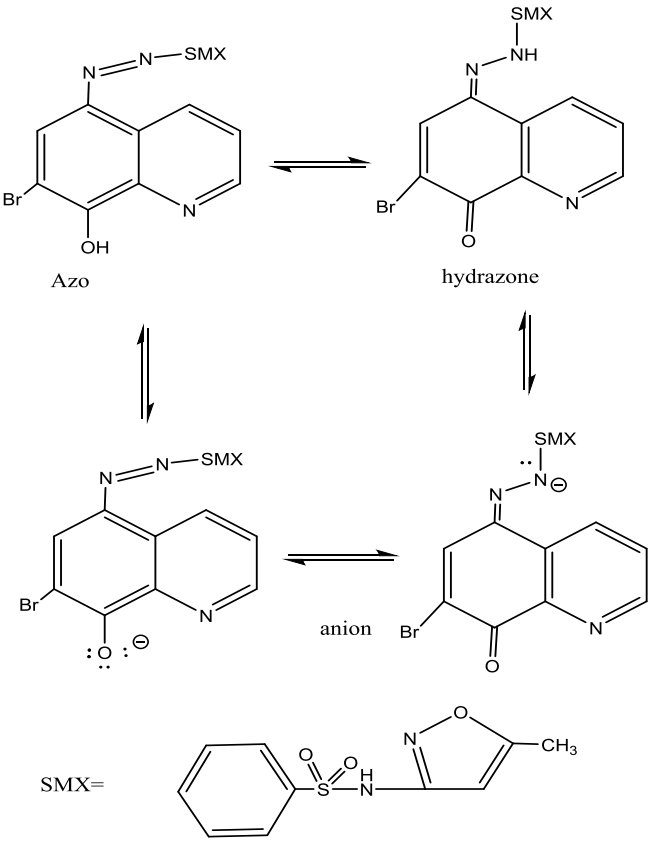

SCHEME 2 Azo-hyrazone tautomeric and anionic for ligand (HAS)

In the spectra of FTIR for the ligand HAS, there was broadband at the range (3380-3244)cm^{-1} for hydroxyl (C8-OH) in quinolone due to forming a very estable hydrogen bond dimer as was depicted in the Scheme 3.The ligand (HAS) institute of five-membered chelate with hydrogen can be assorted into two kinds [13].

1. An inter-molecular hydrogen bonding [O….H-O] resulted from the [C8-OH] moiety and (C8-OH) or nitrogen in (C=N)py for another 7-Bromo 8-HQ.
2. An intra-molecular hydrogen bonding [O-H….N] has appeared between [C8-OH] and nitrogen in (C=N)py in the same 7-Bromo 8-HQ.

In the complexes spectra, this broadband was disappeared and a new band at (1247-1265)cm^{-1} was observed corresponding to (C-O), which indicates the deprotonation of [C_8-OH] for 7-Bromo 8-HQ and acts as monobasic N,O-bidentate ligand [1]. As for (C=N)py the change it was not clear due to interfered with (C=N)iso.

No significant change was noticed in the bands (C-N=N-C), (N=N), (SO_2), and (NH) when comparing the ligand spectrum (HAS) with the complexes spectra indicating not any part of coordination [14,15,1,16].

1) The vibrations of υ $(M-N)_{7\text{-bromo8HQ}}$ and υ(M-O) may be attributed to certain new bands in the ranges of (414-432) and (570-590) cm^{-1} and cm^{-1}, respectively [1]. Figures 2-6 show the results; FTIR spectra data of the bands of ligand (HAS) and their complexes were found in Table 4.

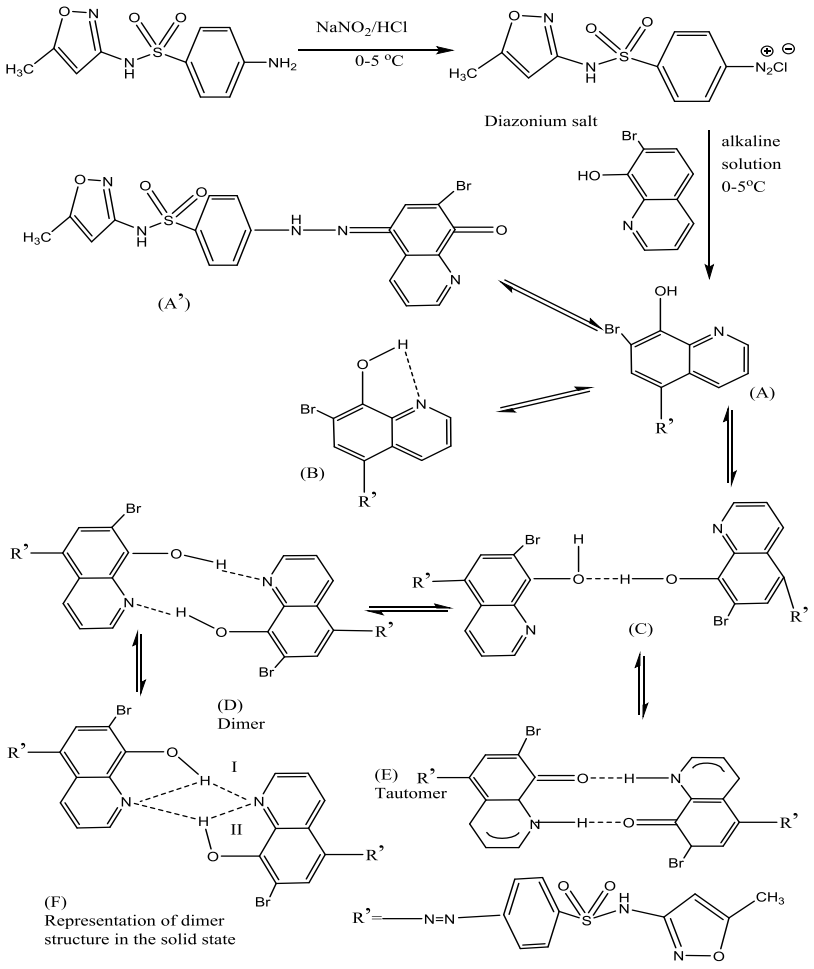

SCHEME 3 hydrogen bond in the ligand (HAS)

TABLE 4 FTIR spectra data for the (HAS) ligand and the complexes

Assessment center	ν (OH)$_{H2O}$ ν(OH)phenolic	ν (N-H)	ν (C=N)iso ν (C=C)imd	ν (C-O)	ν (N=N)	ν (C-N=N-C)	ν (SO_2)	ν (M-N)$_{quinolin}$	ν (M-O)H_2O
HAS	- 3380-3244 br.m	3163 w.	1616 d S. 1595	-	1469 1504 d S.	1398 S.	1336 m	-	-
Co(II)	3317 w. -	3178 w.	1616 m. 1589 w.	1255 m.	1463 1500 d s.	1409 w.	1337 w.	432 w.	574 w.
Ni(II)	3404 m. -	3163 w.	1616 S. 1595 m.	1259 S.	1463 1504 d s.	1409 S.	1330 S.	430 w.	572 w.
Pd(II)	3361 m. -	3163 w.	1616 S. 1591 S.	1247 S.	1463 1502 d S.	1394 S.	1337 S.	418 w.	-
Pt(II)	3313 m. -	3159 w.	1616 S. 1593 S.	1265 w.	1469 d. s 1504 d. s	1396 s.	1338	414 w.	-

w:weak s:strong m:medium d:double t:triple iso: isoxazole imd: imidazole br: broad

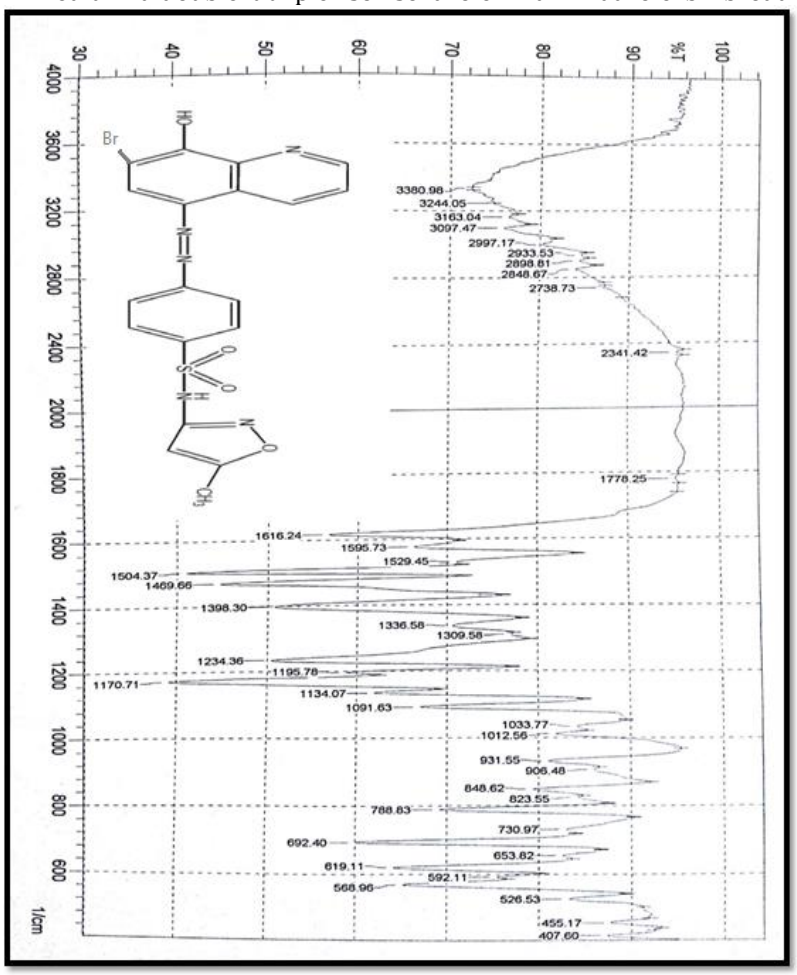

FIGURE 2 FTIR spectrum of HAS ligand

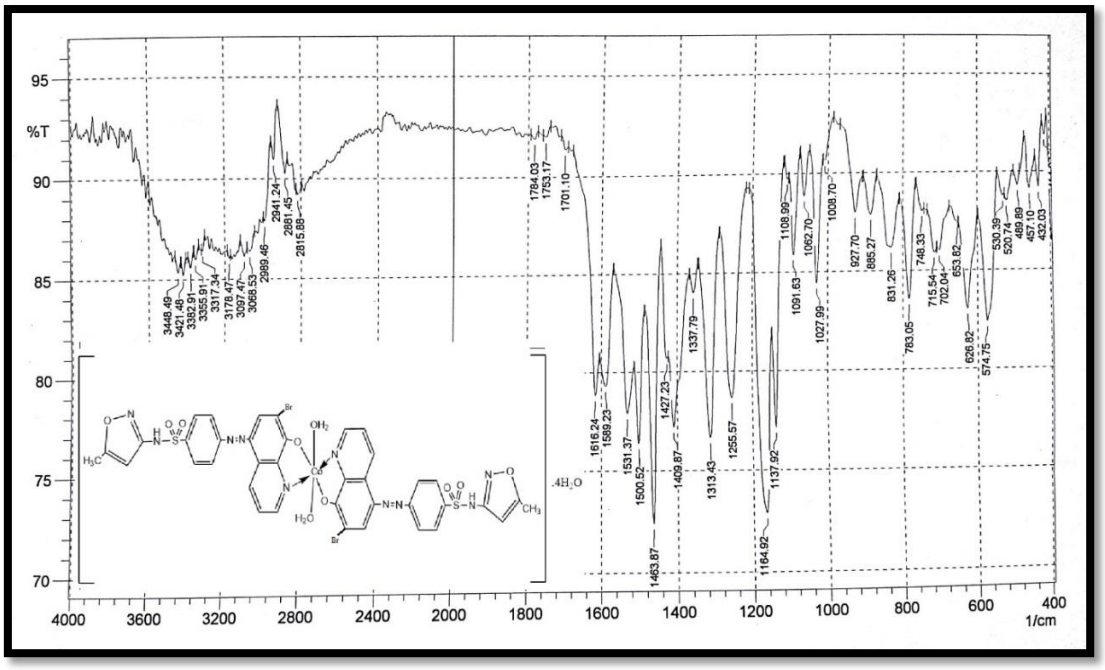

FIGURE 3 FTIR spectrum of $[Co(HAS)_2(H_2O)_2].4H_2O$ complex

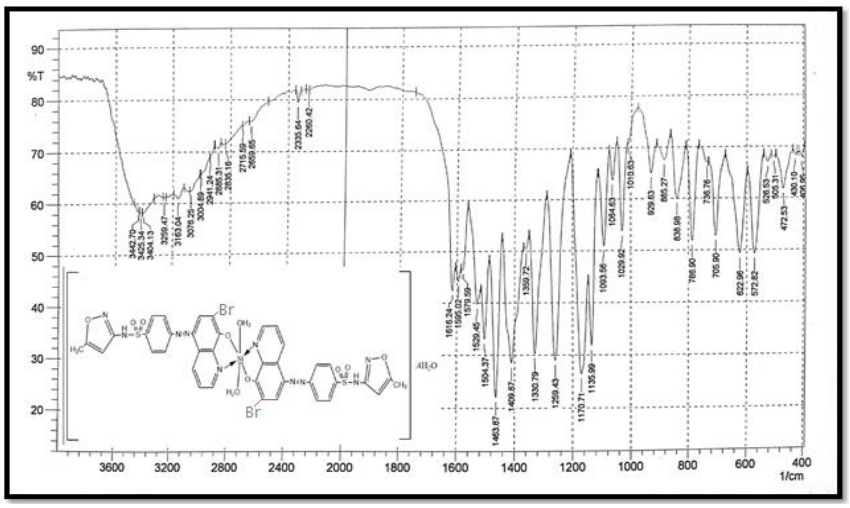

FIGURE 4 FTIR spectrum of $[Ni(HAS)_2(H_2O)_2].4H_2O$ complex

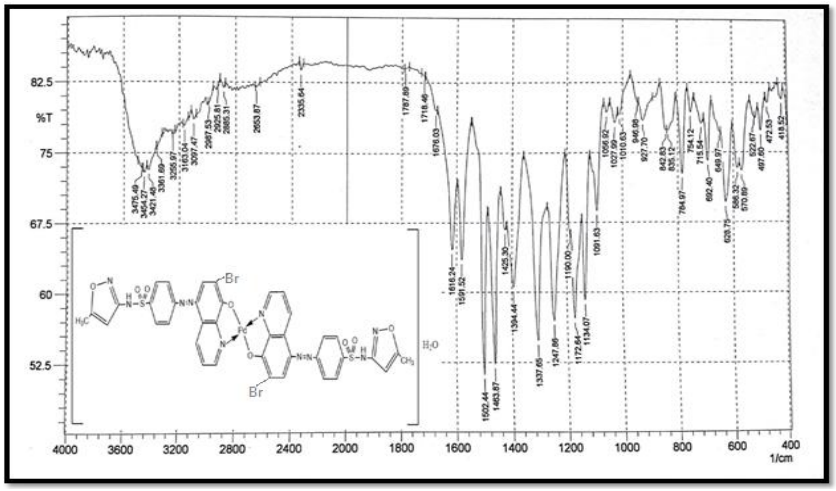

FIGURE 5 FTIR spectrum of $[Pd(HAS)_2].H_2O$ complex

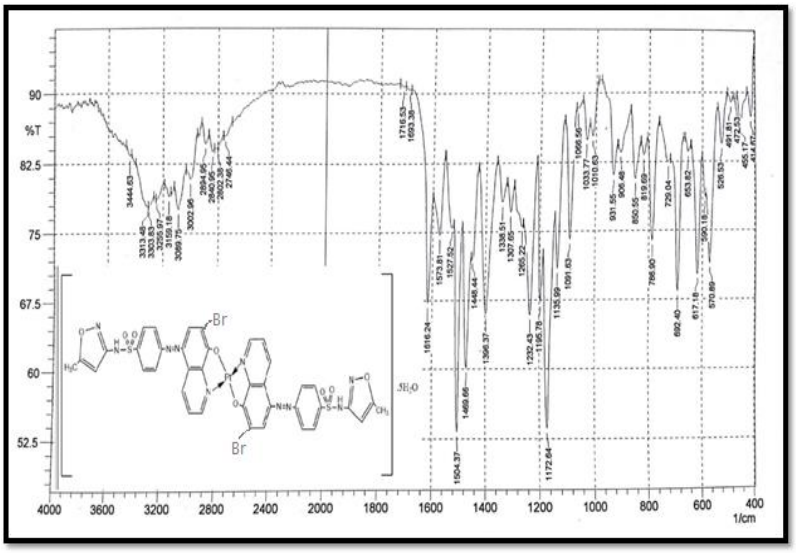

FIGURE 6 FTIR spectrum of $[Pt(HAS)_2].5H_2O$ complex

^{1}H-NMR

The results obtained from the FTIR spectra are further supported by the ^{1}H-NMR analyses. It is accomplished by comparing the changes in the 1HNMR spectra of generated complexes to those of free ligands. Table 5 shows the data for the shifting (δ) in ppm for several kinds of protons in the ligand (HAS) and its complexes for Pt(II) and Pd(II), while the 1HNMR spectra were obtained in DMSO-d6 solution (Figures 7-9).

The free ligand (HAS) shows the signal at (11.65), (2.52) ppm, and the varied signals observed in the range (7.11-8.06) ppm for NHsulfa, CH3oxazole, and Ar-Hbenzene respectively [17]. The free ligand (HAS) displays signals at (9.33)ppm and multiplet signals in the range (8.09-9.03)ppm for OH-quinoline and H-quinoline respectively [18]. All signals of the spectra of complexes of Pd (II) and Pt (II) were a light shift that refers to non-sharing of these groups in metal ions coordination while OH-quinoline signal in the ligand(HAS) is disappeared in the spectra of its complexes indicate sharing oxygen atom with metal ions in the coordination after losing proton [19].

TABLE 5 ^{1}HNMR signals of HAS ligand and the complexes

Comp.	NH_{sulfa}	Ar-$H_{benzene}$	$CH_{3oxazol}$	CH_{oxazol}	$H_{quinoline}$	$OH_{quinoline}$	H_2O
HAS	11.65	7.11-8.06	2.52	6.22	8.09-9.03	9.33	-
$[Pd(HAS)_2].H_2O$	11.64	6.87-7.99	2.52	6.22	8.10-8.28	-	3.37
$[Pt(HAS)_2].5H_2O$	11.62	7.29-7.82	2.51	6.22	8.08-8.39	-	3.55

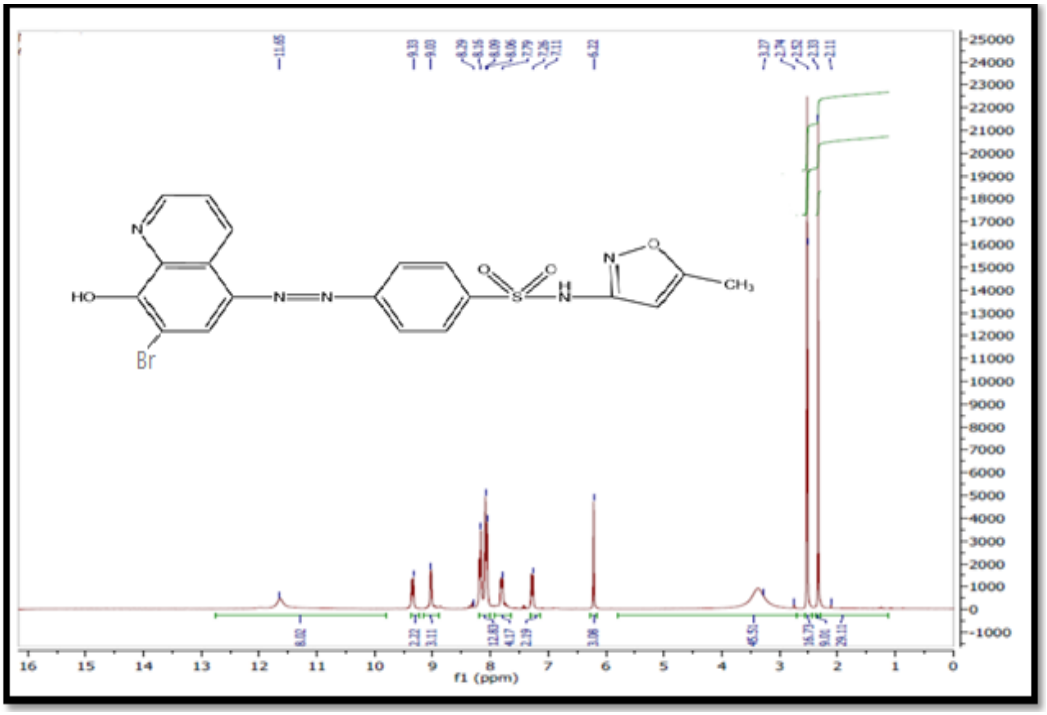

FIGURE 7 Spectrum of ^{1}HNMR for the HAS ligand

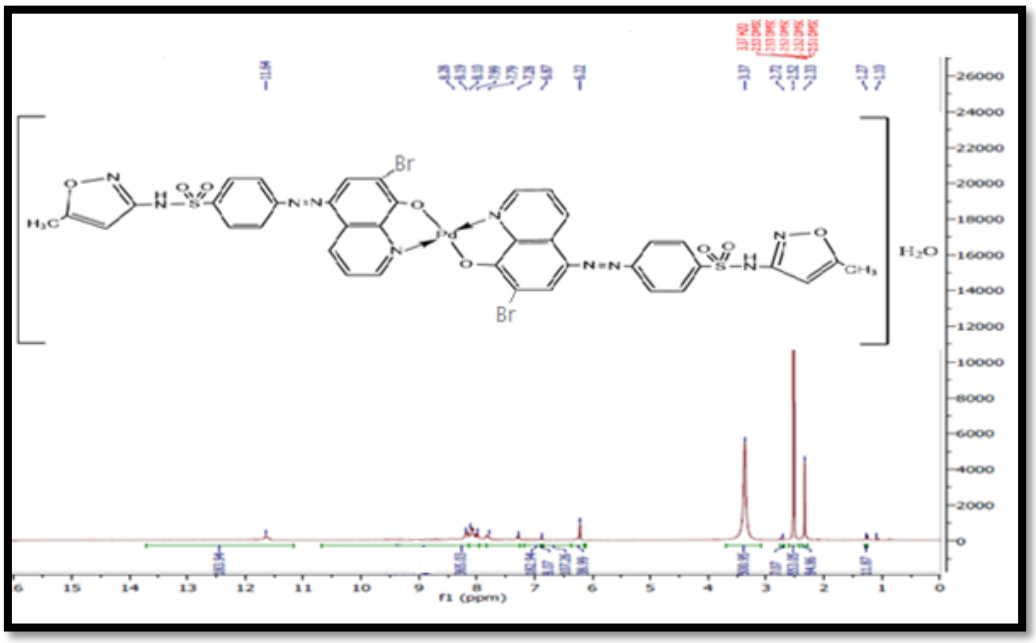

FIGURE 8 Spectrum of ^{1}HNMR for the $[Pd(HAS)_2].H_2O$ complex

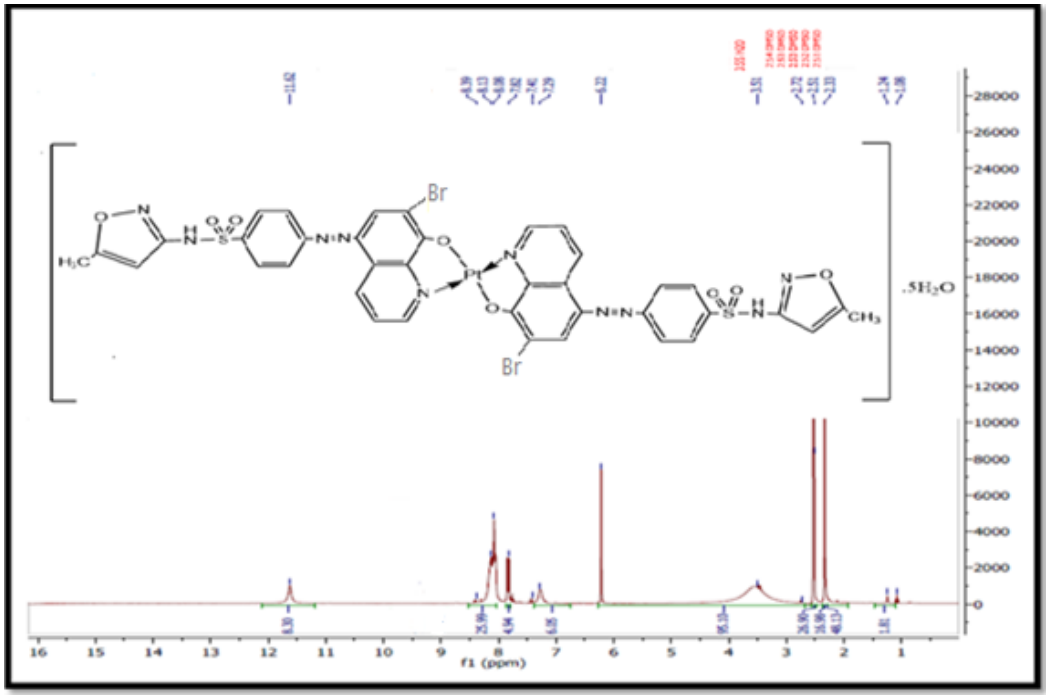

FIGURE 9 Spectrum of ^{1}HNMR for the $[Pt(HAS)_2].5H_2O$ complex

Electronic-spectrum and magnetic properties

The geometry of solid complexes can be determined by looking at their electronic spectra. As a result, electronic spectrum features were concentrated on the discrepancies between the molecule's ground and excited states [20]. Table 6 lists the results of the electronic absorption for the ligand (HAS) and complexes of the ligand within (10^{-4}) molar in ethanol at room temperature, whereas Figures 10-14 explain their spectra. The synthesized complexes' electronic spectra revealed novel bands. The positions and intensities of these bands are primarily determined by depending on the ligand field effect, metal-ion electron configuration, and complex stereochemistry.

The UV-Vis spectrum of the ligand (HAS) in ethanol within the range(200-1100) nm, Figure 10 displays mainly two peaks. The first peak for (HAS) ligand is at (244 nm, 40983 cm^{-1}). This peak was pointed to the mild energy ($\pi \rightarrow \pi^*$) transition of benzene, naphthalene rings. The ($n \rightarrow \pi^*$) transition of intramolecular charge transfer *via* the azo moiety was revealed by the second peak at (405 nm, 24691 cm^{-1}) [21].

In the electronic spectra of para magnetic(2.74)B.M $[Ni(HAS)_2(H_2O)_2].4H_2O$ complex, the (λ_{max}) peak belongs to the ligand (HAS) was shifted as anticipated to higher wave length by (61) nm after coordination. Three d-d transitions were expected for paramagnetic high spin (d^8) octahedral geometry [22].

$\upsilon_1 = {}^3A_2g\ (F) \rightarrow {}^3T_2g\ (F)$
$\upsilon_2 = {}^3A_2g\ (F) \rightarrow {}^3T_1g\ (F)$
$\upsilon_3 = {}^3A_2g\ (F) \rightarrow {}^3T_1g\ (P)$

Figure 11 showed only two weak transitions υ_1 at (893 nm; 11198 cm^{-1}) and υ_2 at (762nm; 13123 cm^{-1}) for the $[Ni(HAS)_2(H_2O)_2].4H_2O$ while the υ_3 transition peak may be cryptic by the (LMCT) peak at (466nm; 21459 cm^{-1})

The complex $[Co(HAS)_2(H_2O)_2].4H_2O$ Figure 12 appears two main transitions:

$\upsilon_1 = {}^4T_1g_{(F)} \rightarrow {}^4T_2g_{(F)}$ at (982 nm; 10183 cm^{-1})
$\upsilon_2 = {}^4T_1g_{(F)} \rightarrow {}^4A_1g_{(F)}$ at (862 nm;11600 cm^{-1})

and also the third transition peak at (496nm; 20161 cm^{-1}) was obscured by the complex

peak[LMCT]. The complex had a distorted octahedral geometry with paramagnetic properties [23].

In the spectra of the diamagnetic low spin (d^8) Pd (II) complex (Figure 13), for square planar surfaces, the three (d-d) transitions were highlighted $^1A_1g \rightarrow {}^1A_2g$, $^1A_1g \rightarrow {}^1B_1g$ and $^1A_1g \rightarrow {}^1E_1g$ [10].

Only two transitions were observed at (971 nm; 10298 cm^{-1} and 839 nm; 11918 cm^{-1}) for $[Pd(HAS)_2].H_2O$ which belongs to $^1A_1g \rightarrow {}^1A_2g$ and $^1A_1g \rightarrow {}^1E_1g$ while the transition $^1A_1g \rightarrow {}^1B_1g$ is too weak to appear. But regarding the peak at (460 nm; 21739 cm^{-1}) was attributed to LMCT.

The value of the magnetic measurement for low spin d^8 Pt(II)- complexes is zero, which is approaching the value of the four-coordinate square planar geometry [24].

Two (d-d) transitions were shown in Figure 14 as explained below $[Pt(HAS)_2].5H_2O$.

$^1A_1g \rightarrow {}^1B_1g$ (742 nm; 13477 cm^{-1})

$^1A_1g \rightarrow {}^1A_2g$ (943 nm; 10604 cm^{-1})

The peak at (443 nm; 22573 cm^{-1}) was attributed to LMCT.

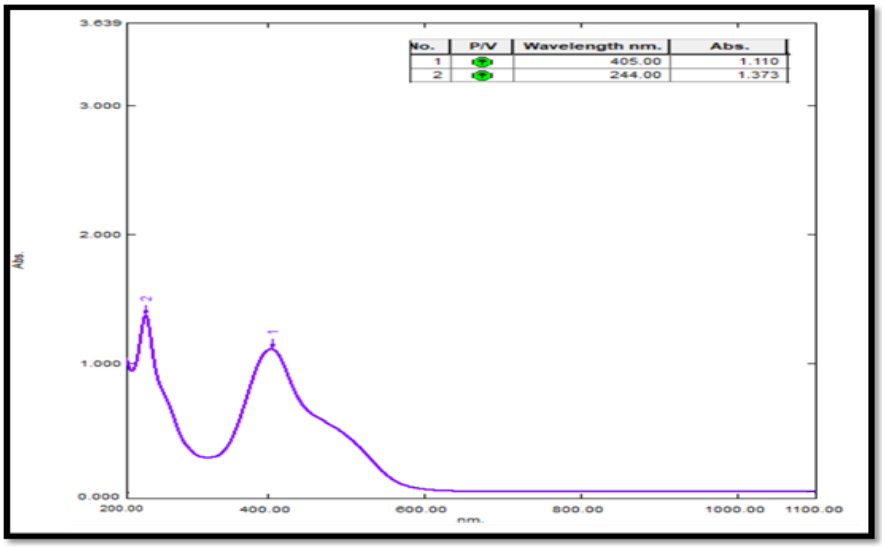

FIGURE 10 The spectrum of UV-Vis of the HAS ligand

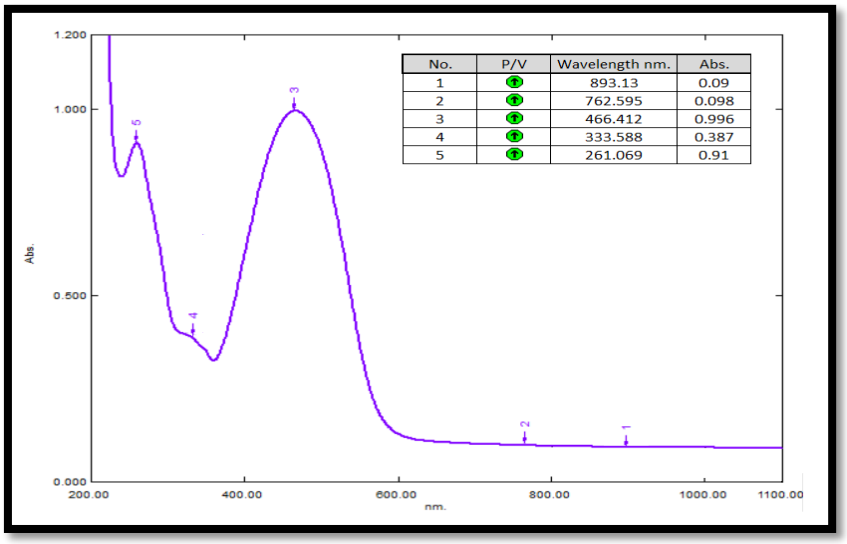

FIGURE 11 The spectrum of UV-Vis of the $[Ni(TAS)_2(H_2O)_2].4H_2O$ complex

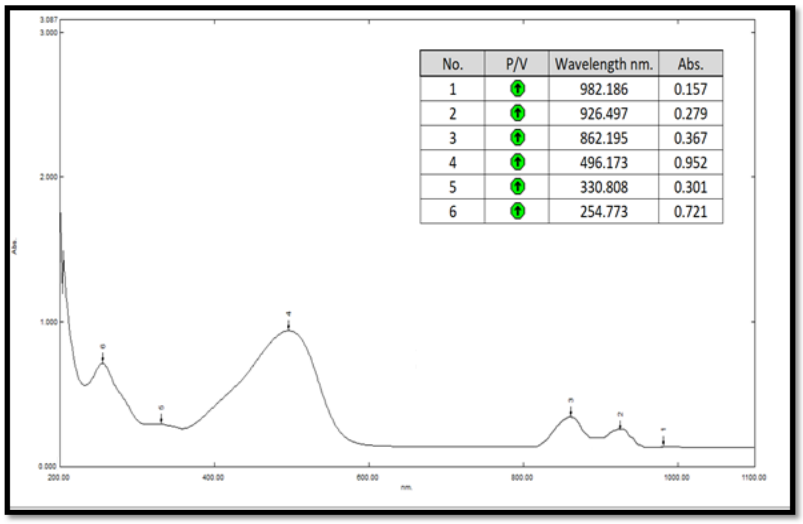

FIGURE 12 The spectrum of UV-Vis of the $[Co(HAS)_2(H_2O)_2].4H_2O$ complex

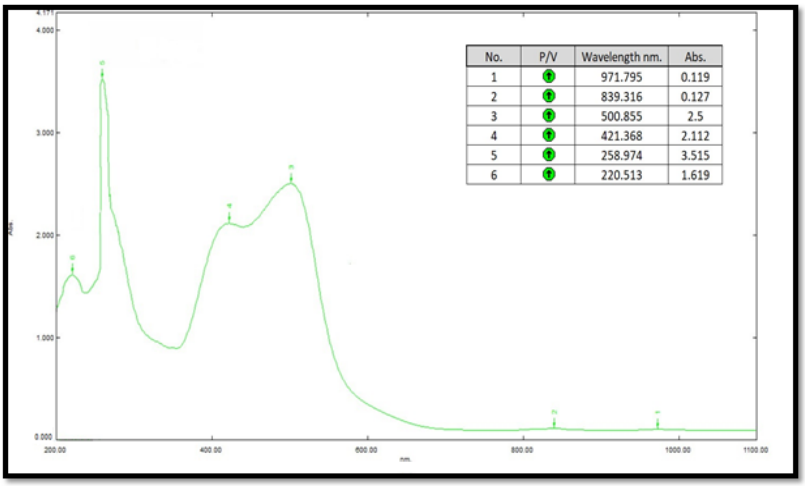

FIGURE 13 The spectrum of UV-Vis of the $[Pd(HAS)_2].H_2O$ complex

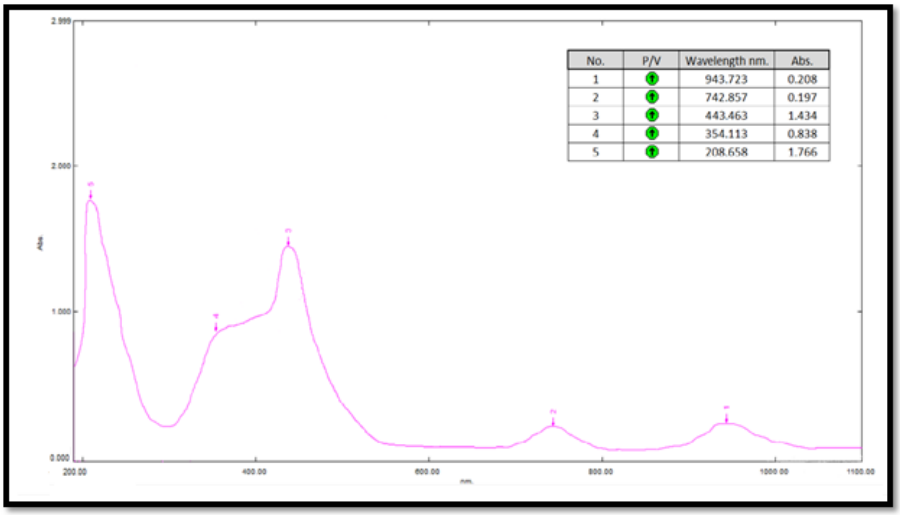

FIGURE 14 The spectrum of UV-Vis of the $[Pt(HAS)_2].5H_2O$ complex

TABLE 6 The ligand (HAS) and its complexes' electronic transition, hybridization, and geometry at (10^{-4}M)

Compound	ƛ(*nm*)	Wavenumber (cm^{-1})	Assignment	hybridization	Geometry	Magnetic properties
HAS	405	24691	n → π*	-	-	-
	244	40983	π → π*			
$[Ni(HAS)_2(H_2O)_2].4H_2O$	893	11198	$^3A_2g_{(F)} \rightarrow {}^3T_2g_{(F)}$	sp^3d^2	octahedral	2.74
	762	13123	$^3A_2g_{(F)} \rightarrow {}^3T_1g_{(F)}$			
	466	21459	LMCT			
	333	30030	n → π*			
	261	38314	π → π*			
$[Co(HAS)_2(H_2O)_2].4H_2O$	982	10183	$^4T_1g_{(F)} \rightarrow {}^4T_2g_{(F)}$	sp^3d^2	Distorted octahedral	3.83
	862	11600	$^4T_1g_{(F)} \rightarrow {}^4A_2g_{(F)}$			
	496	20161	LMCT			
	330	30303	n → π*			
	254	39370	π → π*			
$[Pd(HAS)_2].H_2O$	971	10298	$^1A_1g \rightarrow {}^1A_2g$	dsp^2	Square planer	0.00
	839	11918	$^1A_1g \rightarrow {}^1E_1g$			
	460	21739	LMCT			
	258	38759	π → π*			
	220	45454	π → π*			
$[Pt(HAS)_2].5H_2O$	943	10604	$^1A_1g \rightarrow {}^1B_1g$	dsp^2	Square planer	0.00
	742	13477	$^1A_1g \rightarrow {}^1A_2g$			
	443	22573	LMCT			
	354	28248	n → π*			
	208	48076	π → π*			

Thermo-gravimetric analysis (TGA)

TGA was used to investigate the temperature behavior of the synthesized ligand (HAS) and the complexes (Figures 15-19), while the number of stages changed. Calculated and discovered mass losses are given in Table 7. In our research, the weight loss followed up in the temperature range (25-1000) ^oC and subjected with argon flow. Thermal analysis is used to determine stoichiometry, thermal stability, and whether or not water molecules have crystallized or coordinated. The decomposed species were calculated using the weight losses for each constituent received from the thermal graph [25].

The results can be arranged as follows:

The results and the suggested formulae which is obtained from the analytical data seem to be identical.

1. The thermogravimetric analysis data give an indication that the process of decomposition for the ligand (HAS) is carried out in several steps as well as their complexes.
2. The thermal stability for HAS and its complexes was decreased as in the following order:
3. HAS> $[Ni(HAS)_2(H_2O)_2].4H_2O$ >$[Co(HAS)_2(H_2O)_2].4H_2O$ > $[Pd(HAS)_2].H_2O$ >$[Pt(HAS)_2].5H_2O$

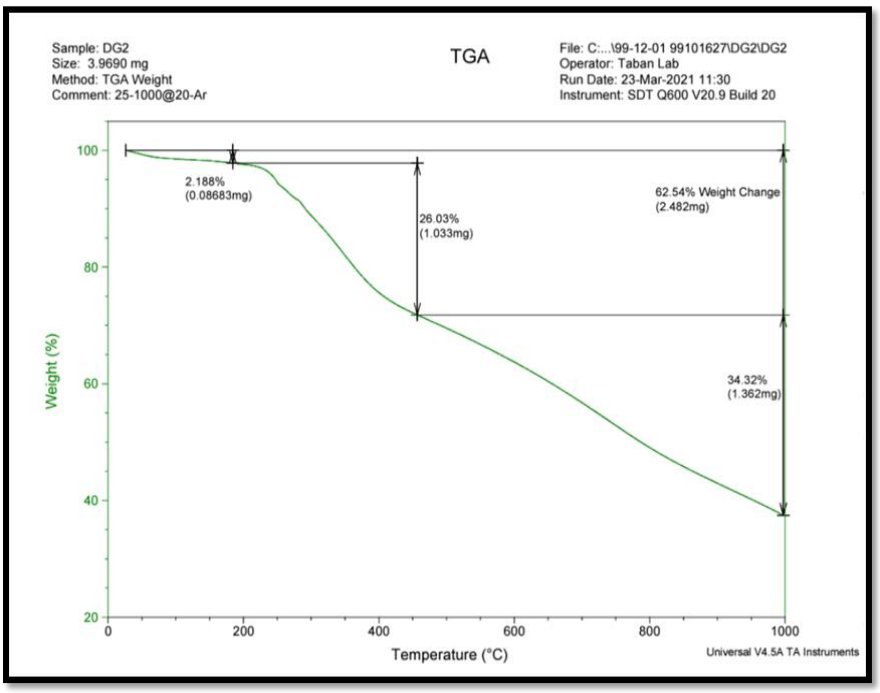

FIGURE 15 Thermogram for the HAS ligand

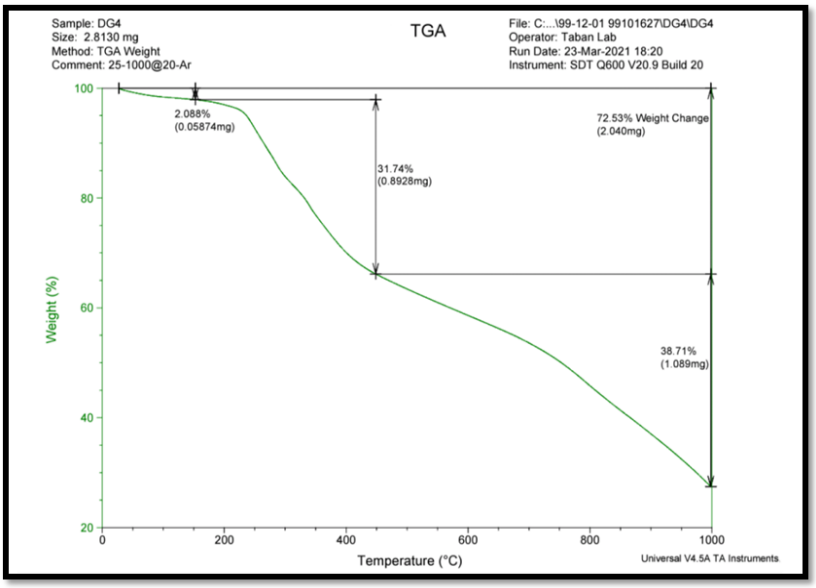

FIGURE 16 Thermogram for $[Pt(HAS)_2].5H_2O$

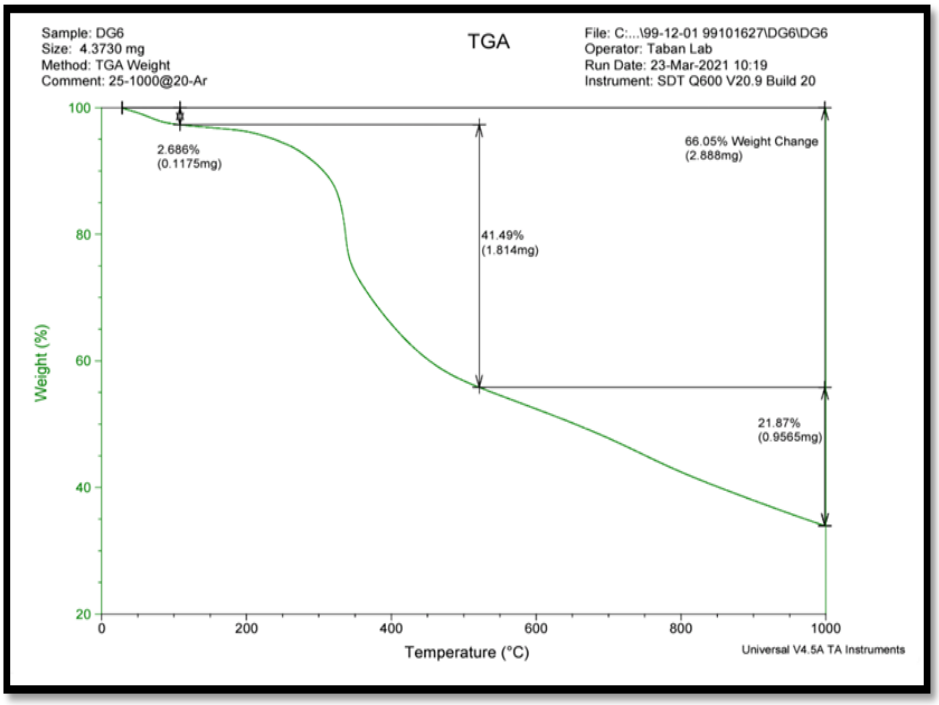

FIGURE 17 Thermogram for the $[Pd(HAS)_2].H_2O$ complex

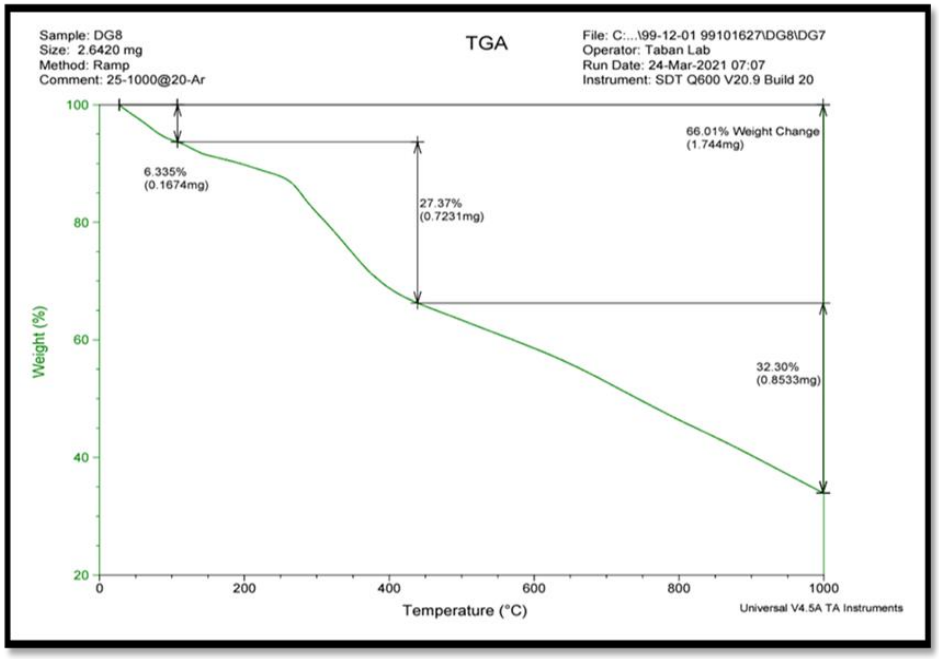

FIGURE 18 Thermogram for the $[Co(HAS)_2(H_2O)_2].4H_2O$ complex

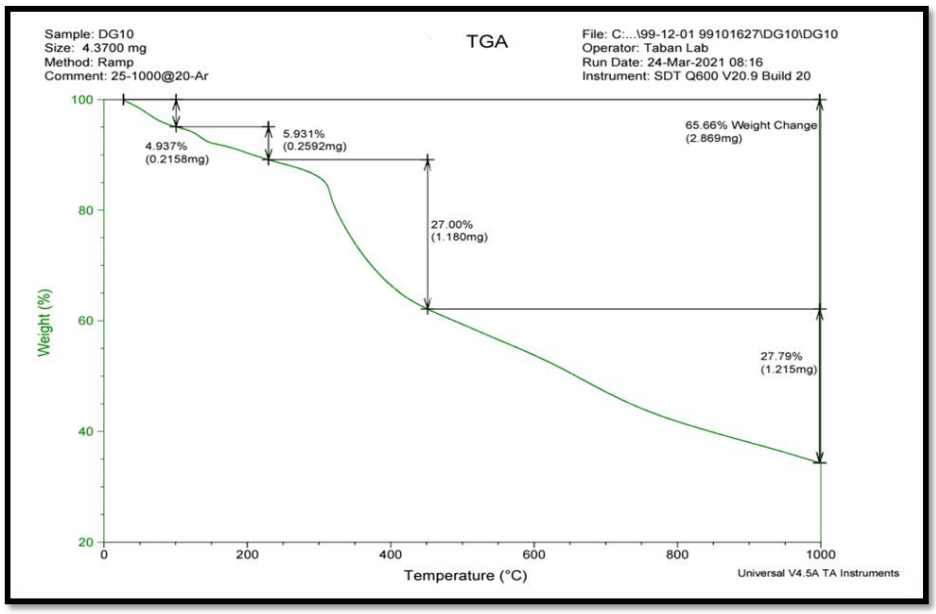

FIGURE 19 Thermogram for the $[Ni(HAS)_2(H_2O)_2].4H_2O$ complex

TABLE 7 TGA of (HAS) ligand and its complexes

Com.	Molecular weight (molecular formula)g/mole	Step	TG. Range of the decompositi on (°C)	Assignment Suggestions	Calculate %	Found %
HAS	$C_{19}H_{14}N_5O_4SBr$ (489.329)	1	(25-180)	$C_{0.5}H_4$	2.188	2.54
		2	(180-450)	$C_{10}H_7$	26.03	25.95
		3	(450-1000)	$C_{8.5}H_3N_{4.5}$	34.32	34.33
		Residue	<1000	$N_{0.5}O_4SBr$	37.46	37.37
$[Pt (HAS)_2].5H_2O$	Pt ($C_{38}H_{38}N_{10}O_{13}S_2Br_2$) (1263.74)	1	(25-150)	H_2O	2.088	1.42
		2	(150-445)	$C_{26}H_{12}Br$	31.74	31.96
		3	(445-1000)	$C_8H_{24}N_{10}O_9Br$	38.71	38.29
		Residue	<1000	$C_4O_3S_2Pt$	27.47	28.09
$[Pd (HAS)_2].H_2O$	Pd ($C_{38}H_{30}N_{10}O_9S_2Br_2$) (1103.078)	1	(25-120)	H_2O	2.68	1.63
		2	(120-530)	$C_{30}H_{20}Br$	41.49	41.69
		3	(530-1000)	$C_8H_8N_4Br$	21.87	21.73
		Residue	<1000	$N_6O_8S_2Pd$	33.95	34.66
$[Co(HAS)_2(H_2O)_2].4H_2O$	Co ($C_{38}H_{40}N_{10}O_{14}S_2Br_2$) (1145.58)	1	(25-110)	$4H_2O$	6.335	6.28
		2	(110-440)	$C_{14}H_{16}O_3Br$	27.37	27.22
		3	(440-1000)	$C_{23}H_{14}Br$	32.30	32.28
		Residue	<1000	$CH_2N_{10}O_7S_2Co$	33.99	33.94
$[Ni(HAS)_2(H_2O)_2].4H_2O$	Ni ($C_{38}H_{40}N_{10}O_{14}S_2Br_2$) (1145.351)	1	(25-100)	$3H_2O$	4.937	4.71
		2	(100-230)	C4H6O	5.93	6.11
		3	(230-450)	$C_{18}H_{14}Br$	27.00	27.05
		4	(450-1000)	$C_{16}H_{14}N_2Br$	27.79	27.4
		Residue	<1000	$N_8O_{10}S_2Ni$	34.34	34.4

Anti-oxidant and radical scavenging activity

Antioxidants help to stabilize a variety of goods, including meals, petrochemicals, medicines, and cosmetics and also help to strengthen an organism's defenses against free radical assaults. It can be found in both

endogenous and exogenous forms in nature [26].

In vitro antioxidant of $[Pt(HAS)_2].5H_2O$ was assessed using reductive ability and DPPH radical scavenging activity. In the reductive ability at all concentration (0.08, 0.16, 0.32, and 0.64) mg/mL for $[Pt(HAS)_2].5H_2O$ was outperformed trolox (control) in the concentration-dependent reductive ability. It was (0.87167 ± 0.001528) at 0.08 mg/mL which was increased significantly to (1.66667 ± 0.005859) at 0.64 mg/mL (Table 8) indicating high reducibility for the complex when compared with trolox.

TABLE 8 Reductive ability of $[Pt(HAS)_2].5H_2O$ and trolox (vitamin E)

Concentration (mg/mL)	Reductive Ability Absorbance (Mean ± SD)	
	$[Pt(HAS)_2]5H_2O$	Trolox (Vitamin E)
0.08	0.87167 ± 0.001528	0.108 ± 0.001^{CD}
0.16	1.0080 ± 0.00200	0.114 ± 0.004^{C}
0.32	1.57433 ± 0.001528	0.132 ± 0.007^{B}
0.64	1.66667 ± 0.005859	0.211 ± 0.015^{A}

There is a lot of interest in creating a new form of synthetic chemical that is less hazardous and has no adverse effects. As a result of the current research using the DPPH test, the metal complex $[Pt(HAS)_2].5H_2O$ was tested for its activity of scavenging. Figure 20 shows the scavenging effect of the tested chemicals at various doses, and it's clear that the action is reliant on coordination among the substances put to the test when compared to standard, the Pt (II) complex had good scavenging action, ascorbic acid used as control [1].

At the five concentrations which were examined (12.5, 25, 50, 100, and 200 mg/mL), $[Pt(HAS)_2].5H_2O$ was substantially more active in DPPH radical scavenging activity than vitamin C. At concentrations of 12.5 mg/mL of $[Pt(HAS)_2].5H_2O$, it was (17.09± 1.857). At 200 mg/mL, DPPH radical scavenging activity increased dramatically to (72.62± 3.981). Table 9 and Figure 20 show the results.

TABLE 9 DPPH radical scavenging activity of $[Pt(HAS)_2].5H_2O$ and vitamin C

Concentration (mg/mL)	DPPH Radical Scavenging Activity (Mean ± SD; %)	
	$[Pt(HAS)_2].5H_2O$	Vitamin C
12.5	17.09 ± 1.857	44.56±1.34
25	27.12 ± 4.513	53.74 ± 2.287
50	40.82 ± 4.693	65.12 ± 5.194
100	52.86 ± 3.050	74.85 ± 1.238
200	72.62 ± 3.981	81.52 ± 3.076

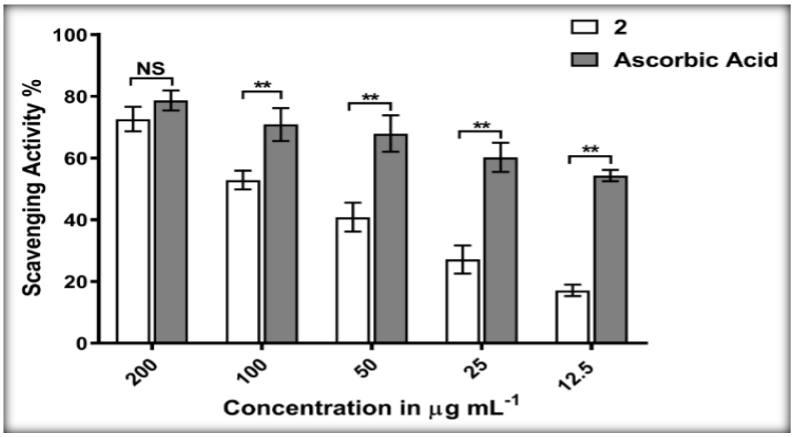

FIGURE 20 Scavenging activity of $[Pt(HAS)_2].5H_2O$

The survey in Anticancer Effectiveness

At the concentration (400 μg/mL), $[Pt(HAS)_2].5H_2O$ had high anti-liver cancer activity. The cytotoxic efficacy was shown to be 60.65% efficient in killing tumor cells. Treatment of HepG-2 cells with $[Pt(HAS)_2].5H_2O$ for 24 hours resulted in a significant rise in cellular metal (Pt) concentration compared to the control (WRL68), suggesting that the complex was easily internalized within 24 hours. MTT test may be used to calculate percentages of dead cells. The cytotoxicity of $[Pt(HAS)_2].5H_2O$ is determined by the cytotoxic impact of Pt(II) conjugated in suppression of HDAC (Histon deacetylases) enzyme, according to the mechanical recommendation covalently binds the positive charge on the histone tail's N-terminal groups of lysine and the phosphor groups in DNA to have a negative charge. The covalent binding of Histone to DNA is critical for gene expression [27].

The half-maximum inhibitory concentration (IC50) is used to determine the efficacy of a medicine. IC50 for the tested substance is (108.3) g/mL during a 24 hours incubation period. As a result, fewer medications are needed to promote cancer cell death, and hence patients can tolerate them Table 10 and Figure 21 show the results after incubation with HepG-2 and WRL68 cells lines for 24 hours at concentrations of (6.25,12.50,25,50,100,200 and 400) μg/mL of the $[Pt(HAS)_2].5H_2O$ complex; modifications of morphological for DNA inclusiveness were performed. Chromatin condensation and nucleus fragmentation with a production of apoptosis and drug resistance were demonstrated by the presence of apoptotic bodies.

TABLE 10 Inhibition activity rate of $[Pt(HAS)_2].5H_2O$ complex *vs* HepG-2 and WRL68

Cell line	Concentration (µg/mL) (Mean and Std. Error of Mean)							IC50 µg/mL	P-value
	400	200	100	50	25	12.5	6.25		
HepG-2	39.35 ±4.78	50.35 ±2.03	63.77 ±3.71	75.27 ±4.26	85.03 ±1.99	95.18 ±1.28	95.95 ±0.53	108.3	<0.0001
WRL-68	66.94 ±6.72	75.54 ±8.43	87.81 ±3.71	95.33 ±1.18	95.22 ±0.82	95.18 ±0.41	95.29 ±1.05	156.5	

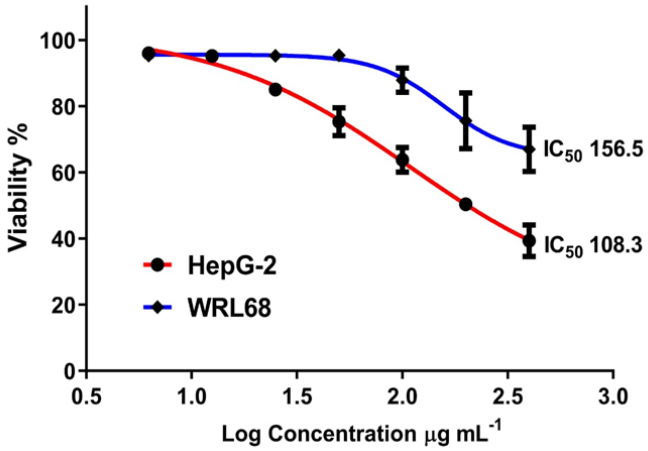

FIGURE 21 Effect of cytotoxicity of $[Pt(HAS)_2].5H_2O$ complex on HepG-2 cells after incubation through 24 hours at 37°C

Antibacterial and antifungal activity for the synthesized ligand and the complexes

Metal (II) complexes are more efficient than free ligands, as indicated in Table 11, indicating that the reactivity of metal ions with the ligand is significant in increasing antibacterial activity. The membrane's lipid that surrounds the cell allows only lipid-

soluble molecules to pass through, making lipo solubility an important component in bacterial activity regulation [29]. The examined compounds' method of action might include forming hydrogen bonds with infected cells' enzyme active sites *via* OH and/or N=N groups and effectively inhibiting them. Furthermore, the chemicals studied have the potential to disrupt organism respiration and impede protein synthesis. Variations in ribosomes in microbial cells or the impermeability of microbes' cells generate differences in the action of various complexes toward distinct species [30]. Finally, the ligand and complexes have effectiveness toward Rhizopus microspores fungi, especially $[Ni(HAS)_2(H_2O)_2].4H_2O$ [31].

The activity increases in this order for *(E.coli)* bacteria : $[Pt(HAS)_2].5H_2O$ > HAS > $[Pd(HAS)_2].H_2O$ > $[Co(HAS)_2(H_2O)_2].4H_2O$ > $[Ni(HAS)_2(H_2O)_2].4H_2O$
and for *(Staph)* bacteria ,the activity increases in this following order : $[Pt(HAS)_2].5H_2O$ > $[Ni(HAS)_2(H_2O)_2].4H_2O$ > HAS > $[Pd(HAS)_2].H_2O$ > $[Co(HAS)_2(H_2O)_2].4H_2O$
while the activity for *Rhizopus microsporus* fungus increases in the following order : $[Ni(HAS)_2(H_2O)_2].4H_2O$ > $[Co(HAS)_2(H_2O)_2].4H_2O$ > and $[Pd(HAS)_2].H_2O$ > HAS > $[Pt(HAS)_2].5H_2O$.

TABLE 11 The scale of zones of inhibition in (mm) of Sulfamethoxazole, fluconazole, ligand (HAS) and the complexes

Comp.	Gram Negative Escherichia coli	Gram Positive Staphylococcus aureus	Rhizopus microsporus
ethanole	---	---	---
sulfamethoxazole	36	38	---
fluconazole	---	---	20
HAS	28	28	15
$[Pt(HAS)_2].5H_2O$	31	38	13
$[Pd(HAS)_2].H_2O$	18	27	16
$[Co(HAS)_2(H_2O)_2].4H_2O$	17	26	21
$[Ni(HAS)_2(H_2O)_2].4H_2O$	13	36	23

Burns healing (anti-inflammatory)
Due to their broad therapeutic usefulness, sulfonamides have become an attractive scaffold. The anti-inflammatory medicines like celecoxib, as well as the antibacterial agents such as sulfamethoxazole and sulfadiazine, are all sulfonamides that are routinely employed as therapeutic agents [32].

The ability of $[Co(HAS)_2(H_2O)_2].4H_2O$ at (1.5) mM silver sulfadiazine (positive control) and negative control to heal burns was investigated by determining the number of days required to recover the results (Table 12), revealed that $[Co(HAS)_2(H_2O)_2].4H_2O$ complex was able to repair burns in 10 days in comparison with what is shown in Figures 22 and 23.

TABLE 12 The recovery of burn healing in mice after different treatments

No. of comp.	Treatment	Period of recovery
1	$[Co(HAS)_2(H_2O)_2].4H_2O$	10 Days
2	Without any treatment	18 Days
3	Silver sulfadiazine	16 Days

FIGURE 22 Mice without any treatment

(a) **(b)**

FIGURE 23 a) Mice with silver sulfadiazine, (b) $[Co(HAS)_2(H_2O)_2]4H_2O$ complex

Performance of dying

Wool fiber includes a variety of polar groups, including –NH, –OH, and–SH groups. An amino group at the end of the chain, as well as a significant number of –NH groups, may be found in polyamide fiber [33].

The type of metal and its valence state, the concentration of a solution, pH, duration, temperature, and other variables, all influence the pace and extent of absorption. The nitrogen atoms of amino and amide groups can form coordination bonds, especially at alkaline pH [34].

Figure 24 showed the wool textile dyeing with the ligand (HAS) and the metal complexes; the color of wool textile were at the range between orange, red and brown.

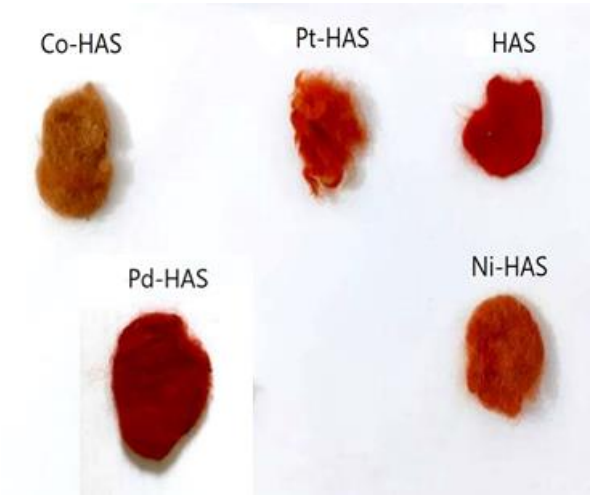

FIGURE 24 The wool textile dyeing of ligand (HAS) with its metal complexes

Wash fastness

Textile color fastness test for washing was carried out using soap with a concentration of 2%, and the results were very good (Table 13).

TABLE 13 Results of dyeing and various fastness feature of azo ligand (HAS) and its complexes on wool textile

Number of compounds	Textile color fatness to wet and dry abrasion		Textile color fatness check for washing	
	Dry rubbing	Wet rubbing	Staining with dye	Color change
HAS	3	3	2	4
(Co-HAS)	4	3	4/5	4
(Ni-HAS)	3/4	3	4	3
(Pd-HAS)	4	4	3	4
(Pt-HAS)	3	3	2/3	3

Grading: 5-4 (good), 3(moderate), 1-2(not good)

Acid - base indicator

Acid-base indicator is a chemical material used to determine if an aqueous solution is acidic, neutral, or alkaline in general. Because acidity and alkalinity affect pH, they are sometimes referred to as pH indicators, and their color changes as the pH changes. Azo dyes are one of the most widely utilized compounds as indicators because they have a squad of delocalization and bright hues, particularly yellow, red, and orange [35].

TABLE 15 Titration of acid (0.1M) against NaOH (0.1M) for (HAS)

No.	Volume of acetic acid	Volume of NaOH	Color in acid	Color in base
1	(HCl) 5 mL	5 mL	orange	Dark orange
2	(ACOH) 5 mL	8.5 mL	orange	red

HAS with HCl **HAS with CH_3COOH**

FIGURE 26 Change in color of Azo ligand (HAS) in acid and base solutions

Conclusion

Based on the findings of spectral and analytical physicochemical investigations for the ligand (HAS) and its complexes, some conclusions have been achieved that lead to establishing the following points:

The ligand (HAS) was synthesized by the diazotization method with some modification and the ligand acted as neutral N, O-bidentate chelating ligand binds to the metal ions of interest. [Co(II), Ni(II), Pt(II), and Pd(II)], through the oxygen and nitrogen atoms of 7-Bromo 8-hydroxyquinoline, form a

pentagonal chelating ring. Pt(II) and Pd(II) complexes are square planar, whereas Ni(II) complex is octahedral and Co(II) complex is distorted octahedral. A water molecule can be either coordination or crystalline. The synthesized complexes were characterized as high stability through examination of the stability constant and hot affected by moisture, light, and heat. Also through thermal analysis, the thermal stability of the produced compounds is shown by TGA. The ligand and the complexes have various anti-bacterial and anti-fungal activities. Some of the complexes are effective as anti-inflammatory, antioxidant, and anticancer. The ligand and the complexes can dye wool fabrics as they have different colors. The ligand (HAS) can change its color depending on the change in pH from acid to base which we can use it as an acid-base indicator.

Acknowledgements

This work was part of a research project of Duaa Jameel Jasim (M.Sc student) in (Science of Inorganic Chemistry, Department of Chemistry, College of Science, University of Baghdad, Baghdad, Iraq). And Supervised by Assistant professor Dr. Alyaa Khider Abbas

Orcid:

Alyaa Khider Abbas: http://orcid.org/0000-0002-8400-0926

References

[1] N.M. Mallikarjuna, J. Keshavayya, M.R. Maliyappa, R.S. Ali, T. Venkatesh, *J. Mol. Struct.*, **2018**, *1165*, 28-36. [crossref], [Google Scholar], [Publisher]

[2] K. Monir, M. Ghosh, S. Mishra, A. Majee, A. Hajra, *Eur. J. Org. Chem.*, **2014**, *2014*, 1096-1102. [crossref], [Google Scholar], [Publisher]

[3] R.F. Dantas, S. Contreras, C. Sans, S. Esplugas, *J. Hazard. Mater.*, **2008**, *150*, 790-794. [crossref], [Google Scholar], [Publisher]

[4] J. Rauseo, A.B. Caracciolo, N. Ademollo, M. Cardoni, M. Di Lenola, W. Gaze, I. Stanton, P. Grenni, T. Pescatore, F. Spataro, L. Patrolecco, *J. Hazard. Mater.*, **2019**, *378*, 120769. [crossref], [Google Scholar], [Publisher]

[5] R. Cherdtrakulkiat, S. Boonpangrak, N. Sinthupoom, S. Prachayasittikul, S. Ruchirawat, V. Prachayasittikul, *Biochem. Biophys. Rep.*, **2016**, *6*, 135-141. [crossref], [Google Scholar], [Publisher]

[6] A.K. Abbas, *Iraqi J. Sci.*, **2015**, *56*, 3297-3309. [Pdf], [Google Scholar], [Publisher]

[7] W. Fu, J. Chen, Y. Cai, Y. Lei, L. Chen, L. Pei, D. Zhou, X. Liang, J. Ruan, *J.Ethnopharmacol.*, **2010**, *130*, 521-528. [crossref], [Google Scholar], [Publisher]

[8] S.D. Sanja, N.R. Sheth, N.K. Patel, D. Patel, B. Patel, *Int. J. Pharm. Pharm. Sci*, **2009**, *1*,74-84. [Google Scholar], [Publisher]

[9] A.K. Abass, **2017**, *28*, 169-186. [Pdf], [Google Scholar], [Publisher]

[10] R.A. Dabish, A.K. Abbas, *Ann. Romanian Soc. Cell Biol.*, **2021**, *25*, 7968-8006. [Pdf], [Google Scholar], [Publisher]

[11] S.A. Abou El-Enein, S.M. Emam, M.W. Polis, E.M. Emara, *J. Mol. Struct.*, **2015**, *1099*, 567-578. [crossref], [Google Scholar], [Publisher]

[12] N.M. Rageh, *Spectrochim. Acta A Mol. Biomol.*, **2004**, *60*, 1917-1924. [crossref], [Google Scholar], [Publisher]

[13] A. Saylam, Z. Seferoğlu, N. Ertan, *J. Mol. Liq.*, **2014**, *195*, 267-276. [crossref], [Google Scholar], [Publisher]

[14] A.Z. El-Sonbati, M.A. Diab, A.A. El-Bindary, A.F. Shoair, N.M. Beshry, *J. Mol. Liq.*, **2016**, *218*, 400-420. [crossref], [Google Scholar], [Publisher]

[15] F.A. Al-Khodir, *Orient. J. Chem.*, **2015**, *31*, 1277-1285. [crossref], [Google Scholar], [Publisher]

[16] A.K. Abbas, R.S. Kadhim, *Orient. J. Chem.*, **2017**, *33*, 402-417. [crossref], [Google Scholar], [Publisher]

[17] N.M. Mallikarjuna, J. Keshavayya, *J. King Saud Univ. Sci.*, **2020**, *32*, 251-259. [crossref], [Google Scholar], [Publisher]

[18] K.D. Patel, H.S. Patel, *Arab. J. Chem.*, **2017**, *10*, S1328-S1335. [crossref], [Google Scholar], [Publisher]
[19] Y. Huo, J. Lu, S. Hu, L. Zhang, F. Zhao, H. Huang, B. Huang, L. Zhang, *J. Mol. Struct.*, **2015,** *1083*, 144-151. [crossref], [Google Scholar], [Publisher]
[20] H.A. Bayoumi, A.M. Alaghaz, M.S. Aljahdali, *Int. J. Electrochem. Sci*, **2013**, *8*, 9399-9413. [Pdf], [Google Scholar], [Publisher]
[21] H. Dinçalp, F. Toker, İ. Durucasu, N. Avcıbaşı, S. Icli, *Dyes Pigm.*, **2007**, *75*, 11-24. [crossref], [Google Scholar], [Publisher]
[22] K.J. Al-Adilee, D.Y. Fanfon, *J. Chem. Chem. Eng.*, **2012**, *6*, 1016. [Pdf], [Google Scholar], [Publisher]
[23] G.G. Mohamed, N.E. El-Gamel, F.A. Nour El-Dien, *Synth. React. Inorg. Met. Org. Chem.*, **2001**, *31*, 347-358. [crossref], [Google Scholar], [Publisher]
[24] K.J. Al-Adilee, K.A. Abedalrazaq, Z.M. Al-Hamdiny, *Asian J. Chem.*, **2013**, *25*, 10475. [crossref], [Google Scholar], [Publisher]
[25] M. Gaber, N. El-Wakiel, O.M. Hemeda, *J. Mol. Struct.*, **2019**, *1180*, 318-329. [crossref], [Google Scholar], [Publisher]
[26] S. Ahmad, M.A. Arshad, S. Ijaz, U. Khurshid, F. Rashid, R. Azam, *Int. Multidiscip. Res. J.*, **2014**, *1*, 41-46. [crossref], [Google Scholar], [Publisher]
[27] A.A. Lane, B.A. Chabner, *Am. J. Clin. Oncol.*, **2009**, *32*, 5459-5468. [crossref], [Google Scholar], [Publisher]
[28] J. Yang, X. Sun, W. Mao, M. Sui, J. Tang, Y. Shen, *Mol. Pharm.*, **2012**, *9*, 2793-2800. [crossref], [Google Scholar], [Publisher]
[29] M. Bouhdada, M.E. Amane, N. El Hamzaoui, *Inorg. Chem. Commun.*, **2019**, *101*, 32-39. [crossref], [Google Scholar], [Publisher]
[30] F.A. Saad, J.H. Al-Fahemi, H. El-Ghamry, A.M. Khedr, M.G. Elghalban, N.M. El-Metwaly, *J. Therm. Anal. Calorim.*, **2018**, *131*, 1249-1267. [crossref], [Google Scholar], [Publisher]
[31] I. Habila, M. Saoudi, F. Berrah, B. Benmerad, M. Boudraa, H. Merazig, S. Bouacida, *J. Mol. Struct.*, **2021**, *16*, 130903. [crossref], [Google Scholar], [Publisher]
[32] H.M. Alshibl, E.S. Al-Abdullah, M.E. Haiba, H.M. Alkahtani, G.E. Awad, A.H. Mahmoud, B.M. Ibrahim, A. Bari, A. Villinger, *Molecules*, **2020**, *25*, 3251. [crossref], [Google Scholar], [Publisher]
[33] M.M. Marie, A.A. Salem, E.M. El Zairy, *J. Text. Inst.*, **2011**, *102*, 790-800. [crossref], [Google Scholar], [Publisher]
[34] F. Ferrero, M. Periolatto, *Ultrason. Sonochem.*, **2012**, *19*, 601-606. [crossref], [Google Scholar], [Publisher]
[35] B. Purwono, C. Anwar, A. Hanapi, *Indones. J. Chem.*, **2013**, *13*, 1-6. [crossref], [Google Scholar], [Publisher]

How to cite this article: Duaa Jameel Jasim, Alyaa khider Abbas. Synthesis, identification, antibacterial, medical and dying performance studies for azo-sulfamethoxazole metal complexes. *Eurasian Chemical Communications*, 2022, 4(1), 16-40. **Link:** http://www.echemcom.com/article_141627.html